Research in Astronomy and Astrophysics, 23:065012 (9pp), 2023 June
https://doi.org/10.1088/1674-4527/accb79

Serpentinisation is Required for the Magnetization of the Martian Crust

Shuoran Yu and Dongdong Ni
State Key Laboratory of Lunar and Planetary Sciences, Macau University of Science and Technology, Macau SAR, China; shuoran.yu@icloud.com
Received 2023 February 25; revised 2023 March 14; accepted 2023 March 20; published 2023 May 23

Abstract

The remnant magnetism in the crust of Martian southern highland is associated with the magnetic sources at an average depth of ∼32 km. In this work, we investigate the magnetization of Martian crust via 1-D parameterized model for the stagnant-lid mantle convection. According to our model, the magnetization of Martian crust is likely to take place in the top-down manner during 4.1–3.7 Ga. To reproduce the average depth of magnetic sources below the southern highland, magnetite and Mg-ferrite are anticipated to be the magnetic carriers in the Martian crust, implying the serpentinisation therein. If magnetite is the only magnetic carrier in the Martian crust, the early climate must be warm enough to maintain a surface temperature of 300 K during 4.1–3.7 Ga at least. Such a warm climate is more likely to be a regional phenomenon associated with the serpentinisation in the crust of the southern highland or the hot ejecta of Borialis impact depositing on the southern hemisphere.

Key words: planets and satellites: interiors – planets and satellites: magnetic fields – planets and satellites: terrestrial planets

1. Introduction

According to the observations of Martian orbital magnetometer, the crust of the Mars, especially the crust of Martian southern highland, was magnetized significantly in the past (Acuna et al. 1999; Connerney et al. 2005; Langlais et al. 2019). The remnant magnetism of Martian crust is a crucial issue for understanding the thermal evolution of the Mars, but its origination was poorly understood. In particular, the carriers of remnant magnetism in the Martian crust are still enigmatic.

The aqueous alteration of olivine and pyroxene, or the so-called serpentinisation, is spoken as a possible mechanism for the generation of magnetic carriers in the Martian crust (Quesnel et al. 2009). In the perspective of chemistry, serpentinisation relates to the hydrous oxidation of ferrous Fe released from the dissolving olivine or pyroxene to ferric Fe in the products and therefore can produce magnetite (McCollom & Bach 2009; McCollom et al. 2022), i.e., an important ferric magnetic carrier in geomagnetism. Based on remote-sensing observations, the outcorps of serpentine were found at several locations on the southern highland associated with Noachian impact craters (Ehlmann et al. 2010; Liu et al. 2023), which may imply the serpentinisation in the early Martian crust. This speculation also provides a plausible explanation for the deep magnetic sources below the southern highland suggested by the spectral analysis on the data of MAVEN magnetometer (Gong & Wieczorek 2021). Besides, the serpentinisation of crust may potentially affect the evolution of planetary climate. Serpentinisation is a source of hydrogen and can promote the abiotic generation of methane (CH_4), i.e., an important greenhouse gas, with the carbon dioxide released from the mantle (Etiope & Sherwood Lollar 2013; Holm et al. 2015; Konn et al. 2015).

In this work, we will use thermal evolution model to examine the magnetization of Martian crust and manifest the necessity of serpentinisation in producing the magnetic carriers in the Martian crust.

2. Methods

The thermal evolution of Martian mantle is modeled by an energy conservation equation coupling the release and absorption of latent heat accompanied with crustal growth and mantle melting, i.e.,

$$\begin{aligned}(1 + \mathrm{St})\,\rho_m c_{pm} V_m \epsilon_m \frac{dT_m}{dt} \\ = -\left[q_{mu} + \left((\rho_{\rm cr} L + \rho_{\rm cr} c_{pcr}(T_m - T_l))\frac{dD_{\rm cr}}{dt}\right)\right] A_l \\ + q_{mb} A_c + \rho_m Q_m V_m \end{aligned} \tag{1}$$

where St is the Stefan number, ρ_m the mantle density, c_{pm} the mantle heat capacity, V_m the volume of the convective mantle, ϵ_m the ratio between the average mantle temperature and the upper mantle temperature, T_m the upper mantle temperature, t the time, q_{mu} the heat flux through the upper boundary layer, $\rho_{\rm cr}$ the crust density, L the specific latent heat, c_{pcr} the crust heat capacity, T_l the lid bottom temperature, $D_{\rm cr}$ the crustal thickness, A_l the area of the lid bottom, q_{mb} the heat flux through the lower boundary layer, A_c the area of the core-mantle boundary (CMB), Q_m the heat production rate of the mantle. The Stefan number is given by

$$\mathrm{St} = \frac{L}{c_{pm} V_m} \int_{V_{\mathrm{melt}}} \frac{d\phi}{dT} dV \tag{2}$$

where L is the specific latent heat, V_{melt} the total volume of melt. The temperature at the bottom of stagnant lid is associated with the mantle temperature via (Grasset & Parmentier 1998)

$$T_l = T_m - \Theta \frac{RT_m^2}{E} \tag{3}$$

where $\Theta = 2.9$ in account of the spherical geometry (Reese et al. 2005).

The heat fluxes through two boundary layers are constrained by the boundary layer theory (Schubert et al. 2001). The thickness of the upper boundary layer is estimated by

$$\delta_{mu} = (r_l - r_c)\left(\frac{\mathrm{Ra}_{mu}}{\mathrm{Ra}_{\mathrm{cr}}}\right)^{-1/3} \tag{4}$$

where r_l is the radius of the lid bottom, r_c the core radius, Ra_{mu} the local Rayleigh number at the upper boundary layer, $\mathrm{Ra}_{\mathrm{cr}}$ the critical Rayleigh number. The local Rayleigh number at the upper boundary layer, i.e.,

$$\mathrm{Ra}_{mu} = \frac{\alpha_m \rho_m^2 c_{pm} g_s \Delta T (r_l - r_c)^3}{K_m \eta_{mu}} \tag{5}$$

where α_m is the thermal expansivity of the mantle, $\Delta T = T_c - T_l$ the temperature difference across the convective mantle, K_m the thermal conductivity of the mantle, η_{mu} the viscosity beneath the upper boundary layer. Correspondingly, the heat flux through the upper boundary layer is given by

$$q_{mu} = K_m \frac{T_m - T_l}{\delta_{mu}}. \tag{6}$$

The thickness of the lower boundary layer is estimated by (Deschamps & Sotin 2000)

$$\delta_{mb} = \left(\frac{K_m \eta_c \mathrm{Ra}_{i,\mathrm{cr}}}{\alpha_m \rho_m^2 c_{pm} g_s (T_c - T_{mb})}\right)^{1/3} \tag{7}$$

where η_c is the viscosity probed in the middle of the lower boundary layer, $\mathrm{Ra}_{i,\mathrm{cr}}$ is the local critical Rayleigh number. The local critical Rayleigh number $\mathrm{Ra}_{i,\mathrm{cr}}$ is given by (Deschamps & Sotin 2000)

$$\mathrm{Ra}_{i,\mathrm{cr}} = 0.28 \mathrm{Ra}_i^{0.21} \tag{8}$$

where $\mathrm{Ra}_i = \alpha_m \rho_m^2 c_{pm} g_s \Delta T_i (r_p - r_c)^3 / K_m \eta_{mu}$ with the planetary radius r_p, $\Delta T_i = (T_m - T_s) + (T_c - T_{mb})$. Then, the heat flux through the lower boundary layer can be determined by

$$q_{mb} = K_m \frac{T_c - T_{mb}}{\delta_{mb}}. \tag{9}$$

According to the adiabatic criteria, the temperature overlying the lower boundary layer can be given by

$$T_{mb} \approx T_m + \frac{\alpha_m g_{mu} T_m}{c_{pm}} (r_l - r_c - \delta_{mu} - \delta_{mb}) \tag{10}$$

where g_{mu} is the gravitational acceleration beneath the upper boundary layer.

The CMB temperature is updated by the energy conservation equation for the core-cooling, i.e.,

$$\rho_c c_{pc} V_c \epsilon_c \frac{dT_c}{dt} = -q_{mb} A_c \tag{11}$$

where ρ_c is the core density, c_{pc} the core heat capacity, V_c the core volume, ϵ_c the ratio between the CMB temperature and the average core temperature, T_c the CMB temperature, A_c the area of the CMB.

The mantle viscosity is constrained by the Arrhenius power-law for the wet mantle (Hirth & Kohlstedf 2003; Tosi et al. 2017), i.e.,

$$\eta = \frac{\eta_r}{X_w^m} \exp\left(\frac{E + pV}{RT} - \frac{E + pV}{RT_r}\right) \tag{12}$$

where η_r is the reference viscosity for the water-free mantle, X_w^m the water content of the solid mantle in ppm, E the activation energy, p the pressure, V the activation volume, R the gas constant, T the temperature, T_r the reference temperature (1600 K).

The growth of stagnant lid relates to the discontinuity of heat flux at the lid bottom. Accounting for the release of latent heat associated with crustal growth, the growth of stagnant lid is constrained by an energy conservation equation at the lid bottom,

$$\begin{aligned} \rho_m c_{pm} (T_m - T_l) \frac{dD_l}{dt} &= -q_{mu} + [\rho_{\mathrm{cr}} L \\ &+ \rho_{\mathrm{cr}} c_{p,\mathrm{cr}} (T_m - T_l)] \frac{dD_{\mathrm{cr}}}{dt} + q_l \end{aligned} \tag{13}$$

where D_l is the thickness of stagnant lid, ρ_{cr} is the crustal density, $c_{p,\mathrm{cr}}$ is the crustal heat capacity, dD_{cr}/dt is the rate of crustal growth, q_l is the heat flux at the lid bottom depending on the heat conduction in the stagnant lid. The temperature in the stagnant lid is modeled by the steady-state heat conduction equation

$$\frac{1}{r^2} \frac{\partial}{\partial r}\left(r^2 K \frac{\partial T}{\partial r}\right) + Q = 0 \tag{14}$$

where Q is the heat production rate. Given the boundary conditions $T(r_p) = T_s$ and $T(r_l) = T_l$, Equation (14) is solved by the linear shooting method.

The growth of Martian crust depends on the supplying of fertile magma from the partially molten mantle. We parameterize the rate of crustal growth by

$$\frac{dD_{\rm cr}}{dt} = \frac{uV_{\rm melt}^{b}}{4\pi r_p^3} \tag{15}$$

where u is the velocity of mantle convection, $V_{\rm melt}^{b}$ is the total volume of buoyant melt. Note that the basaltic magma tends to be non-buoyant in the mantle for the pressures greater than ∼8 GPa (Agee 2008). This point needs to be cautioned for the estimation of $V_{\rm melt}^{b}$. The velocity of mantle convection is parameterized by

$$u = u_0\left(\frac{\rm Ra_{avg}}{\rm Ra_{cr}}\right)^{2/3} \tag{16}$$

where $\rm Ra_{avg}$ is the Rayleigh number estimated by the volumetrically average viscosity of the convective mantle, $u_0 = K_m/(\rho_m c_{pm} r_p)$ is the scale of velocity.

Being geochemically incompatible, the radioactive elements Th, U and K partition into melt accompanied with the melting of Martian mantle, which are brought into the secondary crust at last by the extracted melt. The partitioning of radioactive elements can be described by

$$X_i^{\rm melt} = \frac{X_i^m}{\phi}[1 - (1 - \phi)^{1/d_i}] \tag{17}$$

where the subscript i indicates the element, $X_i^{\rm melt}$ is the concentration of radioactive element in the melt, X_i^m is the concentration of radioactive element in the solid mantle, d_i is the partitioning coefficient. Correspondingly, the average concentration of radioactive element in the uprised fertile magma is

$$\overline{X}_i^{\rm melt} = \frac{1}{V_{\rm melt}}\int_{V_{\rm melt}} X_i^{\rm melt}\phi dV. \tag{18}$$

We constrain the mass of radioactive element in the secondary crust by

$$\frac{dM_i^{\rm scr}}{dt} = \overline{X}_i^{\rm melt}\cdot\frac{dM_{\rm scr}}{dt} = 4\pi r_p^2\rho_{\rm cr}\overline{X}_i^{\rm melt}\cdot\frac{dD_{\rm cr}}{dt} \tag{19}$$

where $M_i^{\rm scr}$ is the mass of radioactive element in the secondary crust, $M_{\rm scr}$ the mass of secondary crust. Then, the concentrations of radioactive element in the crust and mantle are determined as

$$X_i^m(t) = \frac{M_{i,0}^m - M_i^{\rm scr}(t)}{M_m} \tag{20}$$

$$X_i^{\rm cr}(t) = \frac{M_{i,0}^{\rm cr} + M_i^{\rm scr}(t)}{M_{\rm cr}} \tag{21}$$

where $M_{i,0}^m$ is the initial mass of i in the mantle, $M_{i,\rm cr,0}$ is the initial mass of i in the crust.

The partitioning of water also follows Equation (17), but the water content in the melt is limited by a saturation point (Katz et al. 2003), i.e.,

$$X_{w,\rm sat}^{\rm melt} = \chi_1 p^\lambda + \chi_2 p \tag{22}$$

where $\chi_1 = 12.0$ wt%/GPa$^{-\lambda}$, $\chi_2 = 1.0$ wt%/GPa, $\lambda = 0.6$ are three empirical coefficients, p is the pressure (unit: GPa). Hence, the actual water content in the melt should be given by $X_w^{\rm melt} = \min(X_w^{\rm melt}, X_{w,\rm sat}^{\rm melt})$.

The volumetric fraction of melt is modeled by

$$\phi = \frac{T - T_{\rm sol}}{T_{\rm liq} - T_{\rm sol}} \tag{23}$$

where $T_{\rm sol}$ is the solidus temperature, $T_{\rm liq}$ is the liquidus temperature. By taking into account the influences of water, the solidus and liquidus of the mantle are parameterized by (Katz et al. 2003)

$$T_{\rm sol}(p, D_{\rm cr}, X_w^{\rm melt}) = T_{\rm sol,dry}(p) + \Delta T_{\rm sol}(D_{\rm cr}) - k_w X_w^{{\rm melt}\,\gamma_w} \tag{24}$$

$$T_{\rm liq}(p, X_w^{\rm melt}) = T_{\rm liq,dry}(p) - k_w X_w^{{\rm melt}\,\gamma_w} \tag{25}$$

where p is the pressure in GPa, $T_{\rm sol,dry}$ and $T_{\rm liq,dry}$ are the solidus temperature and liquidus temperature of the dry Martian mantle, $\Delta T_{\rm sol}$ is the change of solidus temperature caused by the depletion of mantle, $k = 43$ K/wt% and $\gamma = 0.75$ are two empirical constants (Katz et al. 2003). The solidus temperature and liquidus temperature of the dry Martian mantle are modeled by the data of KLB-1 peridotite (Takahashi 1990), i.e.,

$$T_{\rm sol,dry}(p) = 1409 + 134.2p - 6.581p^2 + 0.1054p^3, \tag{26}$$

$$T_{\rm liq,dry}(p) = 2035 + 57.46p - 3.4872p^2 + 0.0769p^3 \tag{27}$$

where the unit of pressure p is GPa. Accompanied with the extraction of fertile magma, the Martian mantle tends to be more and more depleted. According to the laboratory experiments, the solidus temperature of peridotite can be elevated by ∼150 K by extracting 20 wt% basaltic composition (Maaløe 2004). To couple this effect into thermal evolution model, we parameterize $\Delta T_{\rm sol}$ as a function of crustal thickness by

$$\Delta T_{\rm sol} = \frac{D_{\rm cr}}{D_{\rm ref}}\cdot\Delta T_{\rm sol,ref} \tag{28}$$

$$D_{\rm ref} = f\cdot\frac{r_p^2 - r_c^2}{3r_p^3} \tag{29}$$

where $f = 0.2$ and $\Delta T_{\rm sol,ref} = 150$ K.

Table 1 reports the values of parameters used in the thermal evolution model. Here we consider a Martian core in a radius of 1810 km (Stähler et al. 2021). The densities and thermophysical parameters of Martian crust, mantle and core are set to their typical values. The bulk Th, U and K abundances follow the analysis for SNC meteorites, i.e., $C_{\rm Th} = 56$ ppb, $C_{\rm U} = 16$ ppb and $C_{\rm K} = 305$ ppm, respectively (Wänke & Dreibus 1994).

Table 1
The Values of Parameters in the Thermal Evolution Model

Parameter	Meaning	Value	Unit
r_p	planetary radius	3379	km
r_c	core radius	1810	km
$D_{cr,0}$	initial crustal thickness	0.1	km
ρ_{cr}	crustal density	2900	kg m^{-3}
ρ_m	mantle density	3500	kg m^{-3}
ρ_c	core density	7200	kg m^{-3}
$c_{p,cr}$	crustal heat capacity	1600	J/(kg K)
c_{pm}	mantle heat capacity	1600	J/(kg K)
c_{pc}	core heat capacity	780	J/(kg K)
K_{cr}	crustal thermal conductivity	2.0	W/(m K)
K_m	mantel thermal conductivity	4.0	W/(m K)
α_m	mantle thermal expansivity	3×10^{-5}	K^{-1}
C_{Th}	bulk Th abundance	56	ppb
C_U	bulk U abundance	16	ppb
C_K	bulk K abundance	305	ppm
E	activation energy	300	kJ mol^{-1}
V	activation volume	20×10^{-6}	m^3 mol^{-1}
$\Delta T_{c,0}$	initial core super-heating	300	K
Ra_{cr}	critical Rayleigh number	450	…
d_i	partitioning coefficient of radioactive elements	0.002	…
d_w	partitioning coefficient of water	0.01	…

The initial CMB temperature is super-heated by 300 K with respect to the mantle temperature. The activation energy and activation volume are set to their typical values of peridotite, i.e., 300 kJ mol^{-1} and $\sim 20 \times 10^{-6}$ m^3 mol^{-1}. For the bulk composition of the Mars, the partitioning coefficients of Th, U and K are assigned by 0.002 (Morschhauser et al. 2011). The partitioning coefficient of water is 0.01 (Katz et al. 2003). The reference viscosity η_r, initial mantle temperature $T_{m,0}$ and initial water content $X_{w,0}^m$ are considered as free parameters, which are constrained by reproducing the settings of Martian crustal growth and the present bulk-mantle water content.

The fractional crystallization of Martian magma ocean generated a primitive crust with a thickness of ∼20–30 km before ∼4.5 Ga (Norman 1999; Halliday et al. 2001; Nyquist et al. 2001), but would be reworked soon by the meteorite and asteroid impacts (Humayun et al. 2013; McCubbin et al. 2016). The partial melting in the Martian mantle allows the extraction of fertile magma and the formation of Martian secondary crust since ∼4.5 Ga or earlier time (Bouvier et al. 2018). It is also doubted if the highland crust, which is found to be stratified (Ruiz et al. 2006, 2009), was a combination of primitive crust and secondary crust. Nevertheless, the lower part of the highland crust is speculated to be felsic and may represent a continental crust associated with intrusive activities (Baratoux et al. 2014; Sautter et al. 2015, 2016). Thus, the major part of Martian crust observed at present is more likely to be the secondary crust formed via the extraction of fertile magma from the partially molten Martian mantle, which depends mostly on the thermal evolution of the Mars after the magma ocean phase. In this work, we assume the primitive crust to be destroyed eventually and therefore set an initial crustal thickness of 0.1 km.

3. Results

Previous works suggested several important constraints on the growth of Martian crust. First, geophysical experiments suggest an average crustal thickness of ∼50 km at global scale (Wieczorek & Zuber 2004; Knapmeyer-Endrun et al. 2021). This criterion provides a constraint on the total amount of extracted fertile magma. Second, the growth of Martian crust would have accomplished mostly before the Tharsis rise near the end of Noachian era, i.e., ∼4.0 Ga (Phillips et al. 2001), which provides a constraint for the duration of mantle melting. Third, the observations of gamma-ray spectrum suggests a crustal Th abundance of ∼600 ppb (Taylor et al. 2006). This criterion provides a constraint on the partitioning of radioactive elements during the melting of Martian mantle. In addition to the constraints above, SNC meteorites also indicate a water content of ∼36 ppm in the present bulk Martian mantle (Wänke & Dreibus 1994).

We model the globally averaged case of Martian thermal evolution from 4.5 Ga. The initial mantle temperature, initial bulk-mantle water content, reference viscosity, i.e., the viscosity of water-free Martian mantle at 1600 K, are considered as free variables needing to be constrained by reproducing the four constraints above. The surface temperature depends on the Martian climate and is varied over 220–300 K. Here the lower end-member is the typical average temperature on the present cold Mars, whereas the higher end-member is a habitable temperature and characterizes a warm Mars. As we will show below, the variation of surface temperature can affect the magnetization of Martian crust significantly.

At first, we consider the thermal evolution of the cold Mars with a surface temperature of 220 K. Assuming the primitive crust to be destroyed mostly near ∼4.5 Ga, the settings of Martian crustal growth above and present bulk-mantle water content can be reproduced by an initial mantle temperature of 1670 K, an initial bulk-mantle water content of 70 ppm and a reference viscosity of 9×10^{19} Pa s (Figure 1). Note that the initial mantle temperature and initial bulk water content are basically consistent with those obtained in the previous work, i.e., 1650 K and 100 ppm respectively (Morschhauser et al. 2011). The differences relate to the more realistic wet-mantle rheology used in our model.

As shown in Figure 1(d), the bulk-mantle water extracts rapidly during 4.5–4.0 Ga. In the previous works, the upmost 17–26 km in the Martian crust was suggested to be significantly porous (Hanna & Phillips 2005). As a consequence, a part of mantle-released water can be outgassed further into the Martian

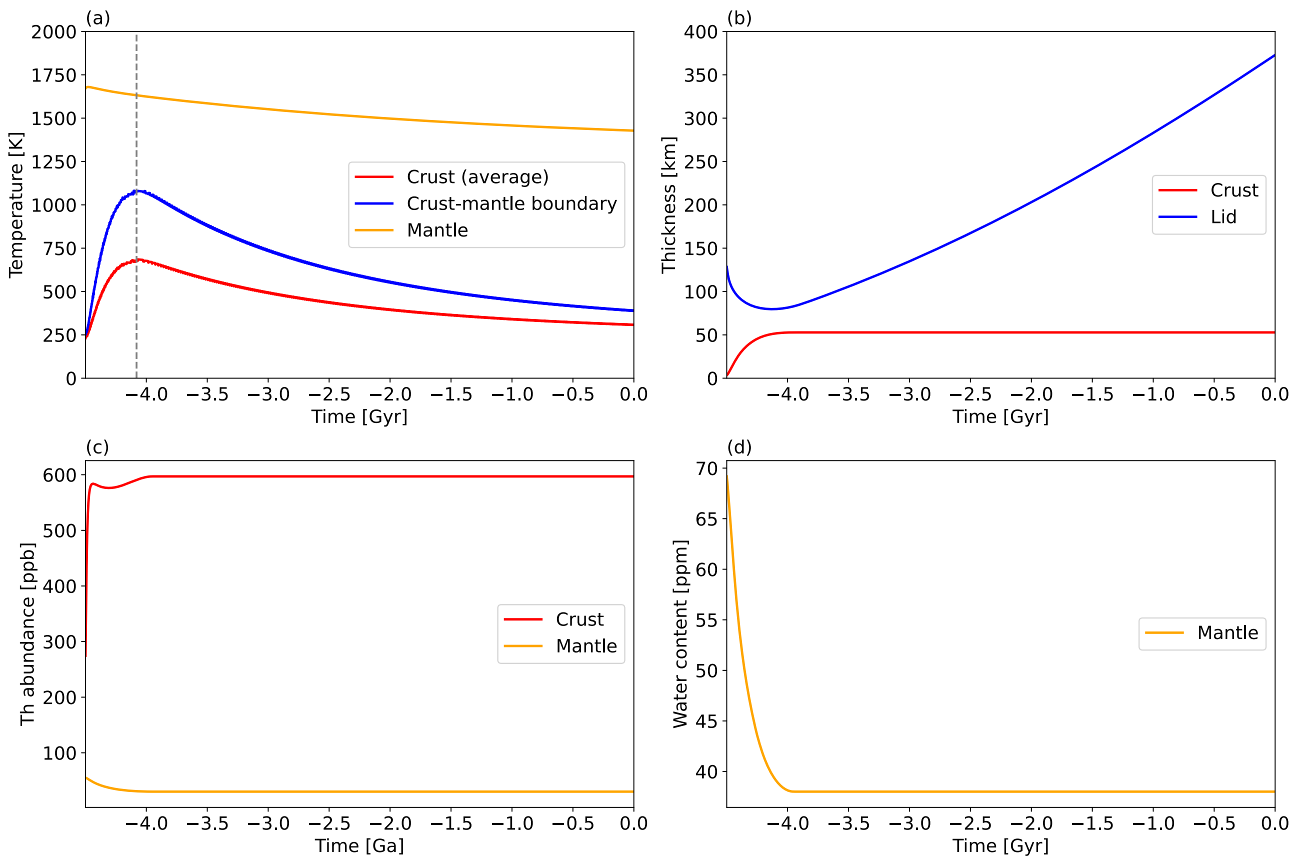

Figure 1. (a) The time evolution of average crustal temperature, crust–mantle boundary temperature and mantle temperature for the cold Mars with a surface temperature of 220 K. The vertical dashed line notes the beginning of crustal cooling at 4.1 Ga. (b) The time evolution of crustal thickness and lid thickness, (c) the time evolution of crustal Th abundance and mantle Th abundance, and (d) the time evolution of bulk-mantle water content. The final crustal thickness, crustal Th abundance and bulk-mantle water content are 52.8 km, 598 ppb and 38 ppm respectively.

atmosphere, whereas the remaining part is likely to deposit in the Martian crust and results in the metamorphism of crustal rocks, including serpentinisation. Correspondingly, the serpentinisation of Martian crust is likely to take place during 4.5–4.0 Ga. We note that this time period just represents the shortest case because the meteorite impacts can also contribute water budget to the bulk Martian crust.

The magnetic carriers can be magnetized when the temperature drops below their individual Curie points. According to Figure 1(a), the Martian crust is heated up before 4.1 Ga, but cools down afterwards. Correspondingly, the magnetization of Martian crust is likely to begin at 4.1 Ga. Besides, the beginning of crustal cooling is close to the end of crustal serpentinisation referred above. Thus, sufficient magnetic carriers should be produced when the Martian crust is able to be magnetized. In order to evaluate the crustal magnetization over depth, we calculate the temperature and pressure profiles in the Martian crust at different times (Figures 2(a) and (b)). Then, we evaluate the demagnetising/magnetizing front (D/MF) based on the Curie point of magnetite (833 K), i.e., a product of serpentinisation (Figure 2(c)). The magnetization begins at the depth of ∼34.7 km at 4.1 Ga. By the end of Martian core dynamo, i.e., ∼3.7 Ga (Mittelholz et al. 2020), the magnetization terminates at the depth of ∼43.3 km. The formed magnetized layer shows an average depth of ∼39 km.

The southern highland is the oldest geologic unit on the Mars and should record most history of crustal magnetization. Based on the spectral analysis on the data of MAVEN magnetometer (Gong & Wieczorek 2021), the magnetic sources in the crust of the southern highland are buried deeply and present an average depth of ∼32 km, shallower than the magnetized layer suggested by our model. There are two possibilities to produce a shallower magnetized layer: (1) the Martian crust contains other magnetic carriers with lower Curie points, and (2) the surface temperature is higher than 220 K. Essentially, serpentinisation relates to the oxidation of ferrous Fe dissolving from olivine and pyroxene to ferric Fe in the water, i.e., $2[Fe^{2+}O] + H_2O = [Fe_2^{3+}O_3] + H_2$. Then, the combination of dissolved ferrous Fe and generated $[Fe_2^{3+}O_3]$ allows the production of magnetite (McCollom & Bach 2009; McCollom et al. 2022). As the other dominant metallic element in olivine and pyroxene, Mg can also be dissolved into water and

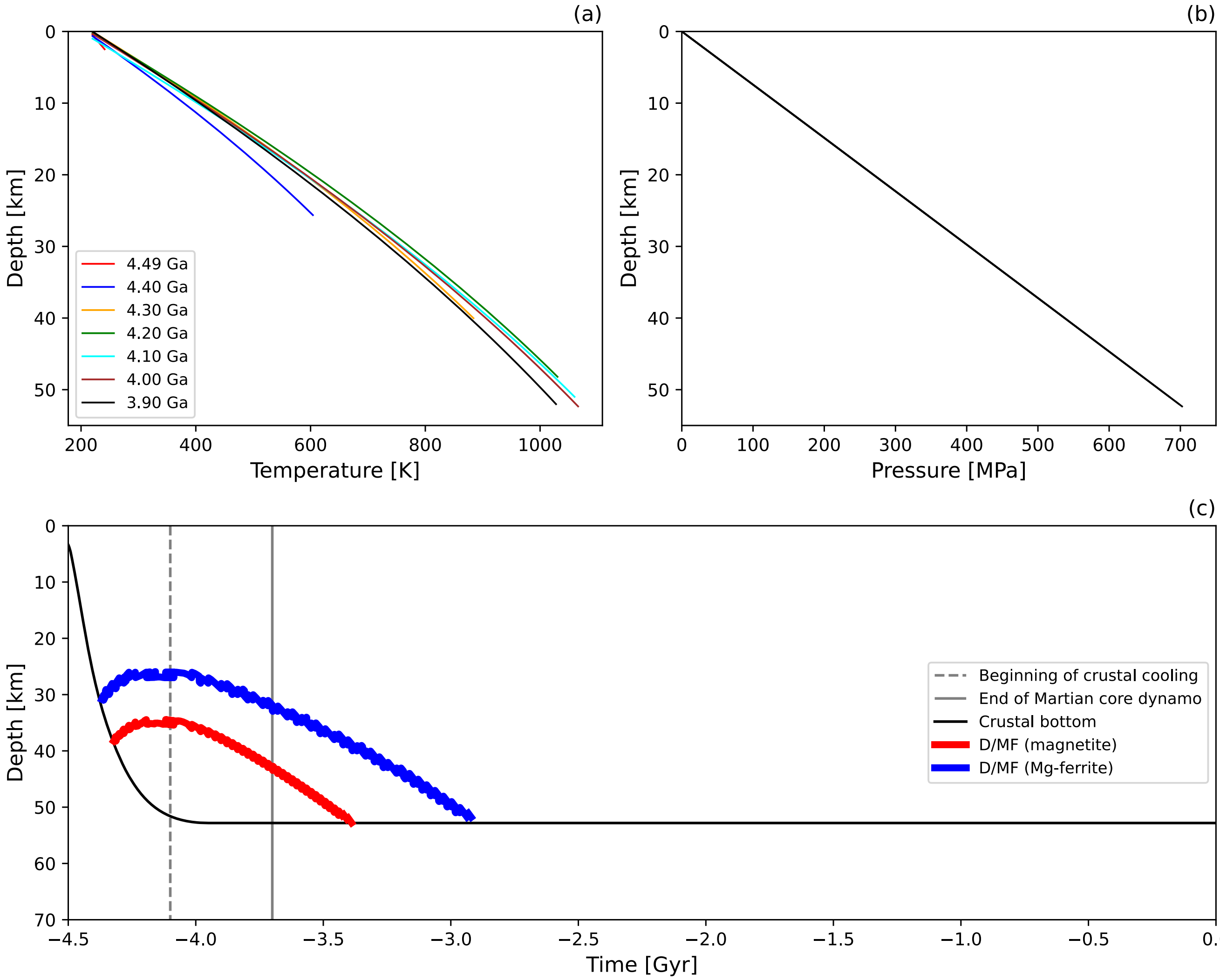

Figure 2. (a) The temperature profiles and (b) the pressure profiles in the crust of the cold Mars with a surface temperature of 220 K. (c) The time evolution of demagnetizing/magnetizing front (D/MF) based on the Curie points of magnetite and Mg-ferrite. The black solid curve notes the crustal bottom. The vertical dashed line notes the beginning of crustal cooling at 4.1 Ga. The vertical solid line notes the end of Martian core dynamo at 3.7 Ga.

combines with the generated [$Fe_2^{3+}O_3$]. Correspondingly, the magnetic carriers produced via serpentinisation is more likely to be $Fe_xMg_{1-x}Fe_2O_4$, where x is a value between zero and one. Here we also consider the magnetization of Mg-ferrite ($MgFe_2O_4$), i.e., the Mg end member of magnetite. Based on the Curie point of Mg-ferrite (713 K), the plotted D/MF suggests a magnetization taking place over the depth of 26.0–32.9 km during 4.1–3.7 Ga (Figure 2(c)). Combining with the magnetized layer associated with magnetite, the Martian crust can be magnetized over the depth of 26.0–43.3 km.

We also consider the thermal evolution of the warm Mars. By a surface temperature of 300 K, the settings of Martian crustal growth and present bulk-mantle water content can be reproduced by an initial mantle temperature 1660 K, a reference viscosity of 8×10^{19} Pa s and an initial bulk water content of 70 ppm (Figures 3(a)–(d)). Here the extraction of bulk-mantle water, as well as the serpentinisation of crustal rocks, occurs mostly during ∼4.5–4.0 Ga. The crustal cooling still begins at ∼4.1 Ga, close to the end of crustal serpentinisation. Thus, the magnetization of Martian crust should begin at ∼4.1 Ga. By treating magnetite as the only magnetic carrier, the magnetization of Martian crust initiates at the depth of ∼30.3 km at ∼4.1 Ga and terminates at the depth of ∼36.9 km at ∼3.7 Ga (Figure 3(e)). The formed magnetized layer shows an average depth of ∼33.6 km, nearly consistent with that below the southern highland.

4. Discussions

Based on the spectral analysis on the data of MAVEN magnetometer, the remnant magnetism in the crust of Martian southern highland, i.e., the oldest geologic unit on the Mars, is

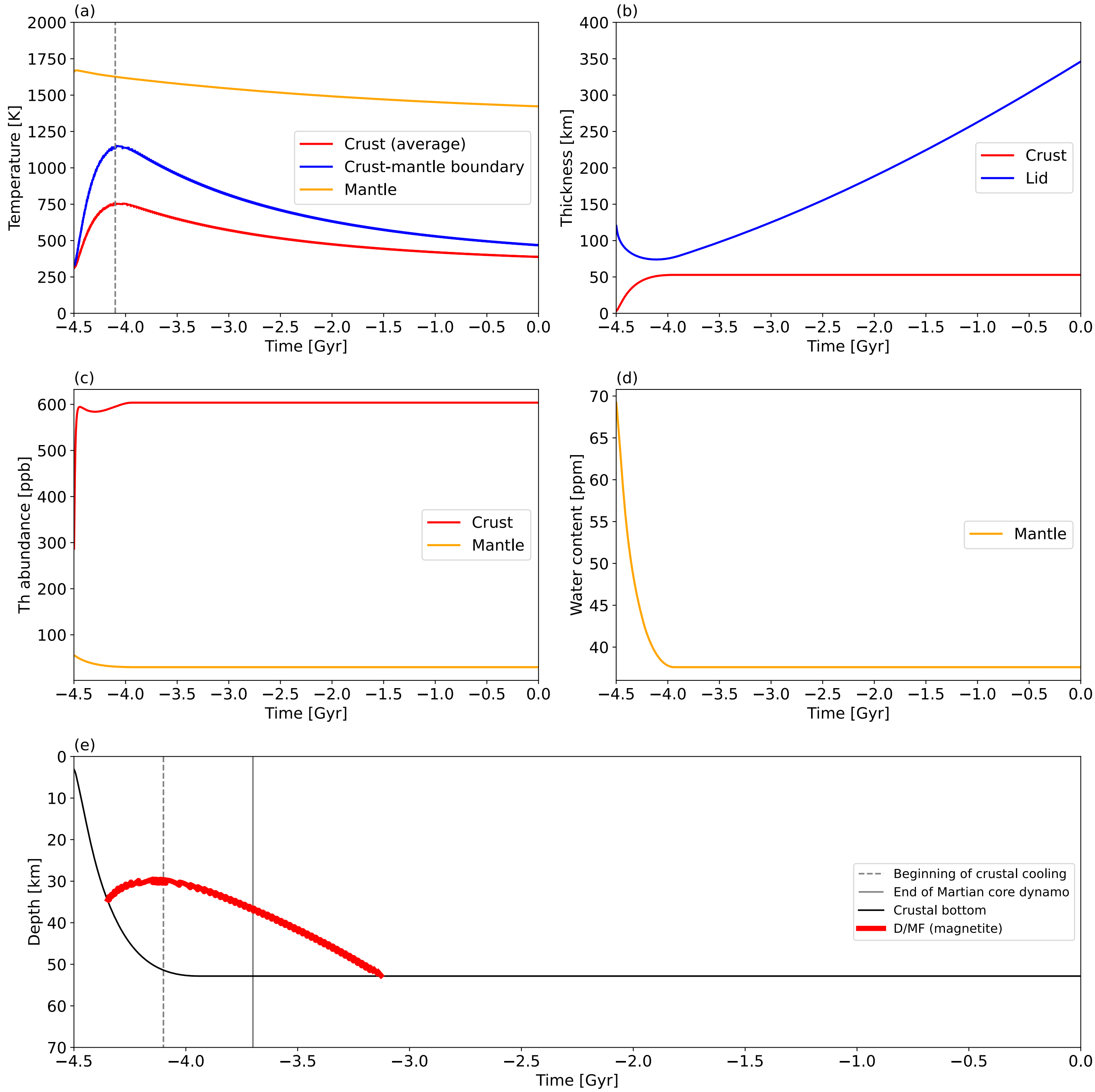

Figure 3. (a) The time evolution of average crustal temperature, crust–mantle boundary temperature and mantle temperature for the warm Mars with a surface temperature of 300 K. The vertical dashed line notes the beginning of crustal cooling at 4.1 Ga. (b) The time evolution of crustal thickness and lid thickness, (c) the time evolution of crustal Th abundance and mantle Th abundance, and (d) the time evolution of bulk-mantle water content. The final crustal thickness, crustal Th abundance and bulk-mantle water content are 52.8 km, 603 ppb and 37 ppm, respectively. (e) The demagnetizing/magnetizing front (D/MF) in the Martian crust evaluated by the Curie point of magnetite.

associated with the magnetic sources at an average depth of ∼32 km (Gong & Wieczorek 2021). According to our thermal evolution model, the magnetization of Martian crust is likely to take place in the top-down manner during 4.1–3.7 Ga. The duration of crustal magnetization is favored by the magnetization of Martian meteorite ALH84001 that occurred during ∼4.1–3.9 Ga (Weiss et al. 2002). For the cold Mars with a surface temperature of 220 K, the average depth of magnetic sources below the southern highland can be reproduced by treating magnetite and Mg-ferrite as the magnetic carriers. For the warm Mars with a surface temperature of 300 K, only magnetite can reproduce the average depth of magnetic sources below the southern highland. Both results favor magnetite as a possible magnetic carrier in the Martian crust, which may imply the serpentinisation therein associated with the deposition of mantle-released water during 4.5–4.0 Ga. Nevertheless, the production of Mg-ferrite via serpentinisation was reported rarely in the previous works and must be verified via the thermodynamic modeling for aqueous alteration.

In the previous works, serpentinisation was studied mainly for the shallow parts in the bulk Earth, e.g., oceanic floors and subduction zones (Christensen 1972), and bulk Mars (McCollom & Bach 2009; McCollom et al. 2022) with pressures up to tens of MPa. In our model, the magnetite needed for explaining the magnetic sources in the Martian crust is anticipated to appear over the depth of 30.3–43.3 km at most, corresponding to the pressures of hundreds of MPa. Thus, the serpentinisation in the Martian crust would involve a high-pressure case, which was reported recently in the studies for the subduction zone of the Earth (Vitale Brovarone et al. 2020).

In the analysis above, we use the depth of magnetic sources below the southern highland as a reference for comparison. Differed from the crust of the southern highland, the remnant magnetism in the crust of the northern lowland is much weaker and relates to the magnetic sources at an average depth of ∼9 km (Gong & Wieczorek 2021). Correspondingly, the formation of the northern lowland is more likely to be a consequence of Borialis impact at ∼4.5 Ga (Andrews-Hanna et al. 2008; Marinova et al. 2008; Nimmo et al. 2008), during which a large amount of magnetic carriers were excavated (Gong & Wieczorek 2021). This hypothesis can well explain the weak remnant magnetism at other impact basins, such as Hellas, Utopia, Argyre and Isidis (Mittelholz et al. 2020), but would be problematic in interpreting the weak remnant magnetism at the northern lowland. In our model, serpentinisation takes place mostly during 4.5–4.0 Ga accompanied with the extraction of bulk-mantle water. Even if the magnetic carriers in the original local crust were excavated substantially at ∼4.5 Ga, the consequential deposition of mantle-released water can still promote the production of magnetic carriers in the remained crust. As a more plausible explanation, Borialis impact might leave a thick melt sheet on the floor of the northern lowland, which in turn changes the local chemical environment, such as composition and oxygen fugacity (Mittelholz et al. 2020). Accordingly, the serpentinisation in the remained crust is likely to be suppressed.

If magnetite is the only magnetic carrier in the Martian crust, the surface temperature must be as high as 300 K to reproduce the result of spectral analysis. Such a high surface temperature would require a warm climate on the Mars, which is controversial with respect to the previous climate models. The valley networks on the Martian southern highland favor the activities of liquid water on the Mars around 3.9–3.6 Ga (Fassett & Head 2008; Hoke & Hynek 2009; Alemanno et al. 2018), but cannot favor a warm early climate conceivably. The liquid water can still persist on the early Mars by a surface temperature below 273 K owing to the low atmospheric pressure and high salinity and acidity of water itself (Fairén 2010). By considering a Martian atmosphere consisting of vapor and carbon dioxide released during the growth of Martian crust, the surface temperature is suggested to be below 273 K during most of Martian history (Grott et al. 2011). In account of these lines of evidences, the long-term warm climate seems to be unlikely on the Mars. Nevertheless, we note that the high surface temperature does not need to be maintained all the time, but is required only during the magnetization of Martian crust, i.e., 4.1–3.7 Ga. Such an episodic warm climate seems to be more compatible with the previous climate models and can be explained by the serpentinisation in the Martian crust. In fact, serpentinisation is a source of hydrogen (McCollom & Bach 2009; McCollom et al. 2022) and can promote the abiotic generation of methane with the mantle-released carbon dioxide, i.e., the so-called Fisher–Tropsch reaction (Holm et al. 2015). As the heat-trapping ability of methane is much stronger than that of carbon dioxide, the produced methane tends to enhance the greenhouse effect on the early Mars. Besides, serpentinisation is also an exothermic process (Früh-Green et al. 2004) and therefore can heat up the early Martian crust and surface. Nevertheless, the crust of the northern lowland, as we referred above, might be serpentinised insignificantly. Hence, the episodic warm climate during 4.1–3.7 Ga is more likely to be a regional phenomenon above the southern highland.

Alternatively, the high surface temperature may also relate to the hot ejecta of Borialis impact depositing on the southern hemisphere, which can maintain the surface temperature above 273 K for up to millions of years (Segura et al. 2002). In such a case, the warm climate is also likely to be a regional phenomenon above the southern highland.

5. Conclusions

The remnant magnetism in the crust of Martian southern highland is associated with the magnetic sources at an average depth of ∼32 km. Based on our thermal evolution model, the Martian crust is likely to be magnetized in the top-down manner during 4.1–3.7 Ga. In order to reproduce the average depth of magnetic sources below the southern highland, magnetite and Mg-ferrite are anticipated to be the magnetic carriers therein. Both ferric oxides would imply the serpentinisation in the Martian crust, which is likely to take place during 4.5–4.0 Ga accompanied with the extraction of bulk-mantle water.

The production of Mg-ferrite via serpentinisation was reported rarely in the previous works and must be verified via thermodynamic modeling for aqueous alteration. If magnetite is the only magnetic carrier in the Martian crust, the surface temperature must be as high as 300 K during 4.1–3.7 Ga at least. Such a high surface temperature may imply a regional warm early climate above the southern highland, perhaps associated with the serpentinisation in the Martian crust or the hot ejecta of Borialis impact depositing on the southern hemisphere.

Acknowledgments

The research for this article was financed by the National Natural Science Foundation of China (Grant No. 12022517), the Science and Technology Development Fund, Macau SAR (File No. 0048/2020/A1), and the Pre-Research Projects on Civil Aerospace Technologies of China National Space Administration (Grant Nos. D020308 and D020303).

ORCID iDs

Shuoran Yu https://orcid.org/0000-0003-0538-5643
Dongdong Ni https://orcid.org/0000-0002-0483-0445

References

Acuna, M., Connerney, J., Ness, N. F., et al. 1999, Sci, 284, 790
Agee, C. B. 2008, RSPTA, 366, 4239
Alemanno, G., Orofino, V., & Mancarella, F. 2018, E&SS, 5, 560
Andrews-Hanna, J. C., Zuber, M. T., & Banerdt, W. B. 2008, Natur, 453, 1212
Baratoux, D., Samuel, H., Michaut, C., et al. 2014, JGRE, 119, 1707
Bouvier, L. C., Costa, M. M., Connelly, J. N., et al. 2018, Natur, 558, 586
Christensen, N. I. 1972, JG, 80, 709
Connerney, J., Acuña, M., Ness, N., et al. 2005, PNAS, 102, 14970
Deschamps, F., & Sotin, C. 2000, GeoJI, 143, 204
Ehlmann, B. L., Mustard, J. F., & Murchie, S. L. 2010, GeoRL, 37, 53
Etiope, G., & Sherwood Lollar, B. 2013, RvGeo, 51, 276
Fairén, A. G. 2010, Icar, 208, 165
Fassett, C. I., & Head, J. W., III 2008, Icar, 198, 37
Früh-Green, G. L., Connolly, J. A., Plas, A., Kelley, D. S., & Grobéty, B. 2004, The Subseafloor Biosphere at Mid-ocean Ridges, Vol. 144 (Washington, DC: American Geoscience Union), 119
Gong, S., & Wieczorek, M. 2021, JGRE, 126, e2020JE006690
Grasset, O., & Parmentier, E. 1998, JGRB, 103, 18171
Grott, M., Morschhauser, A., Breuer, D., & Hauber, E. 2011, E&PSL, 308, 391
Halliday, A., Wänke, H., Birck, J.-L., & Clayton, R. 2001, SSRv, 96, 197
Hanna, J. C., & Phillips, R. J. 2005, JGRE, 110, E01004
Hirth, G., & Kohlstedf, D. 2003, Geophysical Monograph-American Geophysical Union, 138, 83
Hoke, M. R., & Hynek, B. M. 2009, JGRE, 4, 8705
Holm, N. G., Oze, C., Mousis, O., Waite, J., & Guilbert-Lepoutre, A. 2015, AsBio, 15, 587
Humayun, M., Nemchin, A., Zanda, B., et al. 2013, Natur, 503, 513
Katz, R. F., Spiegelman, M., & Langmuir, C. H. 2003, GGG, 4, 1073
Knapmeyer-Endrun, B., Panning, M. P., Bissig, F., et al. 2021, Sci, 373, 438
Konn, C., Charlou, J.-L., Holm, N. G., & Mousis, O. 2015, AsBio, 15, 381
Langlais, B., Thébault, E., Houliez, A., Purucker, M. E., & Lillis, R. J. 2019, JGRE, 124, 1542
Liu, W.-P., Yin, W., Ye, B.-L., et al. 2023, Icar, 369, 114644
Maaløe, S. 2004, MinPe, 81, 1
Marinova, M. M., Aharonson, O., & Asphaug, E. 2008, Natur, 453, 1216
McCollom, T. M., & Bach, W. 2009, GeCoA, 73, 856
McCollom, T. M., Klein, F., & Ramba, M. 2022, Icar, 372, 114754
McCubbin, F. M., Boyce, J. W., Novák-Szabó, T., et al. 2016, JGRE, 121, 2120
Mittelholz, A., Johnson, C., Feinberg, J., Langlais, B., & Phillips, R. 2020, SciA, 6, eaba0513
Morschhauser, A., Grott, M., & Breuer, D. 2011, Icar, 212, 541
Nimmo, F., Hart, S., Korycansky, D., & Agnor, C. 2008, Natur, 453, 1220
Norman, M. D. 1999, M&PS, 34, 439
Nyquist, L., Bogard, D., Shih, C.-Y., et al. 2001, in Chronology and Evolution of Mars: Proc. of an ISSI Workshop (Bern: Springer), 105
Phillips, R. J., Zuber, M. T., Solomon, S. C., et al. 2001, Sci, 291, 2587
Quesnel, Y., Sotin, C., Langlais, B., et al. 2009, E&PSL, 277, 184
Reese, C., Solomatov, V., & Baumgardner, J. 2005, PEPI, 149, 361
Ruiz, J., Tejero, R., & McGovern, P. J. 2006, Icar, 180, 308
Ruiz, J., Williams, J.-P., Dohm, J. M., Fernández, C., & López, V. 2009, Icar, 203, 47
Sautter, V., Toplis, M., Wiens, R., et al. 2015, NatGe, 8, 605
Sautter, V., Toplis, M. J., Beck, P., et al. 2016, Litho, 254, 36
Schubert, G., Turcotte, D. L., & Olson, P. 2001, Mantle Convection in the Earth and Planets (Cambridge: Cambridge Univ. Press)
Segura, T. L., Toon, O. B., Colaprete, A., & Zahnle, K. 2002, Sci, 298, 1977
Stähler, S. C., Khan, A., Banerdt, W. B., et al. 2021, Sci, 373, 443
Takahashi, E. 1990, JGRB, 95, 15941
Taylor, G. J., Boynton, W., Brückner, J., et al. 2006, JGRE, 111, E03S10
Tosi, N., Godolt, M., Stracke, B., et al. 2017, A&A, 605, A71
Vitale Brovarone, A., Sverjensky, D., Piccoli, F., et al. 2020, NatCo, 11, 3880
Wänke, H., & Dreibus, G. 1994, RSPTA, 349, 285
Weiss, B. P., Vali, H., Baudenbacher, F. J., et al. 2002, E&PSL, 201, 449
Wieczorek, M. A., & Zuber, M. T. 2004, JGRE, 109, E01009